



A Unified Nonlinear Fiber-Based Framework for Predicting Axial–Flexural Interaction in Reinforced Concrete Shear Walls

Islam Ibrahim Shoheb^{1,*}, Moustafa Metwally², Intan Rohani Endut²

¹Technical Manager, MAS Engineering and Construction Company Ltd., KSA

²Graduate School of Management (GSM), Management and Science University, Shah Alam, Malaysia

Emails: Eslamshohip03@gmail.com; 012024021443@gsm.msu.edu.my; Intan_rohani@msu.edu.my

Abstract

Purpose - Reinforced concrete (RC) shear walls are critical lateral-load resisting elements; however, reliable prediction of their axial–flexural interaction behavior remains difficult, particularly for irregular geometries and nonuniform reinforcement layouts. This study aims to develop an accurate and versatile analytical framework to evaluate the global axial–flexural response of RC shear walls. **Design/methodology/approach** - A fully nonlinear, code-independent numerical framework is formulated based on strain compatibility, equilibrium enforcement, and curvature-controlled sectional analysis. The model incorporates advanced stress–strain relationships for confined and unconfined concrete, a bilinear steel constitutive law, and a high-resolution fiber discretization scheme capable of representing arbitrary cross-sectional shapes. The framework generates complete moment–curvature responses and axial–moment (P–M) interaction diagrams under uniaxial bending. **Findings** - The results exhibit strong agreement with established analytical models and reported experimental trends. The framework accurately captures nonlinear degradation, neutral-axis migration, confinement effects, and the influence of reinforcement distribution on axial–flexural capacity. **Practical implications** - The proposed model provides a reliable tool for performance-based assessment, design, and optimization of RC shear walls beyond simplified code provisions. **Originality/value** - The study introduces a geometry-independent, fully nonlinear modeling approach that enables detailed evaluation of irregular RC shear walls with enhanced accuracy and practical applicability.

Keywords: Axial-flexural behavior; Confined concrete; Fiber modelling; Interaction diagrams; Nonlinear analysis; Reinforcement optimization; Shear walls

1. Introduction

Reinforced concrete (RC) shear walls are widely recognized as the primary lateral-load resisting components in mid- and high-rise structures, where their axial–flexural response directly governs strength, ductility, and seismic performance [1–3]. Subjected simultaneously to gravity loads and overturning moments, shear walls exhibit complex axial–moment (P–M) interaction behavior that must be accurately quantified to support performance-based design, capacity evaluation, and structural reliability assessment [3–5]. Consequently, understanding axial–flexural interaction remains a central research topic in reinforced concrete structural engineering.

Axial–flexural interaction critically influences stress redistribution, neutral-axis migration, and transitions between compression-controlled, balanced, and tension-controlled failure modes [1,6]. Under seismic loading, fluctuations in axial force significantly affect compression block development, reinforcement engagement, and deformation capacity [7,8]. Despite extensive prior research, most existing analytical and design-oriented models remain constrained by simplified assumptions, regular rectangular geometries, or code-dependent formulations, limiting their applicability to contemporary structures characterized by irregular wall shapes and nonuniform reinforcement layouts [5,9,10]. Furthermore, many studies isolate individual parameters—such as geometry, reinforcement ratio,

or confinement—without offering a unified framework capable of evaluating interaction behavior across a broad range of configurations [11,12].

A rigorous assessment of axial–flexural behavior necessitates a strain-compatibility-based formulation that enforces plane-section behavior, nonlinear material response, and equilibrium between internal and external forces [6,13]. Although strain compatibility is well established at the sectional level, its systematic extension to arbitrary wall geometries, variable reinforcement distributions, and full axial load spectra remains insufficiently addressed in the literature [5,8]. In addition, reinforcement layout has a decisive influence on wall performance; however, prevailing design practices rely largely on prescriptive detailing rules rather than optimization-based evaluation, leaving the effects of reinforcement distribution on capacity efficiency and ductility degradation inadequately quantified [7,11,12,14].

Motivated by these limitations, this study proposes a fully nonlinear, code-independent numerical framework for evaluating the axial–moment interaction behavior of RC shear walls. The methodology is founded on generalized strain compatibility and employs high-resolution sectional discretization to accommodate arbitrary geometries and nonuniform reinforcement layouts under varying axial load conditions. The framework explicitly tracks neutral-axis migration, captures nonlinear material behavior, and integrates a reinforcement optimization strategy aimed at improving strength efficiency while remaining consistent with international design principles. The resulting P–M interaction envelopes provide a unified representation of wall behavior across the entire interaction domain. The key findings demonstrate that the proposed framework accurately captures established analytical trends and essential behavioral mechanisms governing RC shear wall response. The outcomes offer practical value to researchers, practicing engineers, and code developers seeking advanced tools for performance-based assessment and design of irregular shear wall systems. The remainder of this paper is organized as follows: the numerical formulation and material models are presented first, followed by verification and parametric investigations, discussion of results, and concluding remarks highlighting practical implications and future research directions.

2. Literature Review

2.1 Classical Background of Axial–Flexural Interaction

Early investigations into axial–flexural interaction in reinforced concrete members modeled shear walls analogously to columns using simplified stress–strain representations. The nonlinear concrete compression model introduced by Hognestad [15] laid the foundation for sectional analysis under combined axial load and bending. Building on this work, Bresler and Gilbert [16] formalized axial–moment interaction concepts, which later became integral to the development of interaction diagrams for reinforced concrete members.

Classical reinforced concrete theory, as presented by Park and Paulay [17] and later consolidated by MacGregor and Wight [18], adopted strain compatibility and simplified equivalent rectangular stress blocks as the analytical basis for most code-oriented interaction models. While these formulations have proven effective for regular rectangular sections, their simplifying assumptions restrict their ability to capture nonlinear material behavior, neutral-axis migration, and stress redistribution in walls with irregular geometries or nonuniform reinforcement layouts. Consequently, their applicability to modern shear wall configurations remains limited.

2.2 Experimental Insights into Shear Wall Behavior

Experimental research has provided essential insight into the influence of axial load on shear wall strength, ductility, and failure mechanisms, as illustrated in Figure 1. Early experimental programs by Hidalgo et al. [19] identified distinct flexural, shear, and mixed failure modes governed primarily by axial load ratio and wall slenderness. Lefas et al. [20] further demonstrated that increasing axial compression enhances flexural strength but significantly reduces deformation capacity, as shown in Figure 2. These findings highlighted the inherent trade-off between strength and ductility under elevated axial loads.

Paulay and Priestley [1] emphasized the critical role of boundary confinement in improving curvature capacity and seismic performance, particularly under high axial compression. Subsequent full-scale cyclic tests conducted by Thomsen and Wallace [12] confirmed the strong sensitivity of ductility demand and failure mode to axial load magnitude and boundary reinforcement detailing. While experimental studies offer valuable physical understanding, their high cost, limited specimen numbers, and restricted parametric coverage constrain systematic evaluation of geometry, reinforcement layout, and axial–flexural interaction across a broad design space.

2.3 Strain-Compatibility-Based Numerical Approaches

Strain compatibility has emerged as a widely accepted numerical approach for evaluating axial–flexural capacity due to its clear physical basis and computational efficiency. The confined concrete constitutive model proposed by Mander et al. [21] significantly enhanced strain-compatibility-based predictions under high compression levels

by incorporating confinement effects explicitly. For shear wall applications, sectional and fiber-based models employing strain compatibility have been validated against experimental data, demonstrating accurate prediction of boundary compression strains and neutral-axis migration [23]. These studies confirmed the capability of strain compatibility to capture nonlinear behavior across compression-controlled, balanced, and tension-controlled interaction regimes. However, most existing implementations remain either geometry-specific, tailored to particular wall shapes, or embedded within code-dependent frameworks, limiting their general applicability and transferability to irregular wall systems.

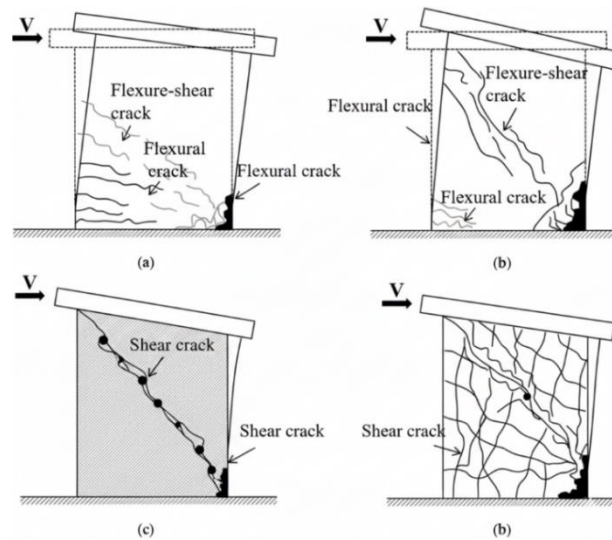


Figure 1. Typical failure modes of RC shear walls under combined axial load and bending: (a) flexure-dominated at low axial load, (b) shear-dominated at high axial load, and (c) mixed flexural–shear behavior.

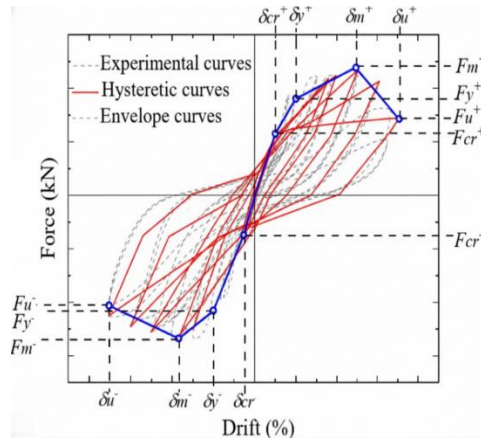


Figure 2. Effect of axial load ratio on RC shear wall cyclic response: increased strength accompanied by reduced deformation capacity and earlier strength degradation.

2.4 Effects of Geometry and Reinforcement Distribution

Wall geometry plays a decisive role in axial–flexural interaction behavior. Studies on flanged and non-rectangular walls reported asymmetric stress redistribution, enhanced flexural capacity, and increased sensitivity to axial load variations [12,22]. Experimental investigations on U-shaped and other irregular wall configurations revealed pronounced neutral-axis shifts and asymmetric hysteretic responses, underscoring the inadequacy of simplified interaction models for such systems [22].

Reinforcement distribution further governs shear wall performance. Concentrated boundary reinforcement has been shown to improve confinement efficiency and flexural strength, whereas uniformly distributed reinforcement often leads to inefficient material utilization [12]. Despite recognition of these effects, most previous studies examine geometry and reinforcement independently, and reinforcement optimization is rarely integrated within a comprehensive axial–moment interaction framework.

2.5 Limitations of Code-Based and Finite Element Approaches

Design standards such as ACI 318 and Eurocode 2 provide simplified axial–moment interaction formulations primarily intended for preliminary design [1]. Although practical, these code-based relationships are generally conservative and inadequate for irregular geometries or performance-based seismic assessment [1,12]. Advanced finite element models can simulate shear wall behavior in detail; however, they are often associated with high computational cost, sensitivity to constitutive assumptions, and limited suitability for extensive parametric or optimization-driven studies [23]. These drawbacks restrict their practicality for routine design evaluation and comparative assessment of multiple wall configurations.

2.6 Identified Research Gap

The reviewed literature indicates that, despite significant advances, no unified, geometry-independent, and code-independent numerical framework currently exists that can systematically evaluate axial–flexural interaction for arbitrary shear wall geometries, explicitly track neutral-axis migration, and incorporate reinforcement distribution within an efficient computational scheme. This deficiency represents a critical gap in current research and design practice.

2.7 Position of the Present Study

The present study addresses this gap by proposing a generalized strain-compatibility-based numerical framework for predicting the axial–moment interaction behavior of RC shear walls. The framework is fully nonlinear, geometry-independent, and capable of accommodating nonuniform reinforcement layouts, enabling efficient generation of complete P–M interaction envelopes suitable for advanced analysis and performance-based design applications.

3. Research Methodology

3.1 Method of data collection

This study adopts a quantitative, computational research methodology to develop and validate a comprehensive, fully nonlinear numerical framework for predicting the global axial–flexural interaction behavior of reinforced concrete (RC) shear walls. The methodology integrates: (a) nonlinear material constitutive modeling, (b) fiber-based sectional discretization, (c) strain compatibility and equilibrium enforcement, (d) iterative neutral-axis determination, (e) moment–curvature analysis, and (f) systematic generation of axial–moment (P–M) interaction envelopes. The framework is intentionally code-independent, relying exclusively on fundamental mechanics and nonlinear constitutive relationships rather than specific provisions of ACI, Eurocode 2, or ECP. This ensures international applicability and facilitates unbiased comparison across diverse wall configurations. A schematic overview of the complete numerical workflow is presented in Figure 3.

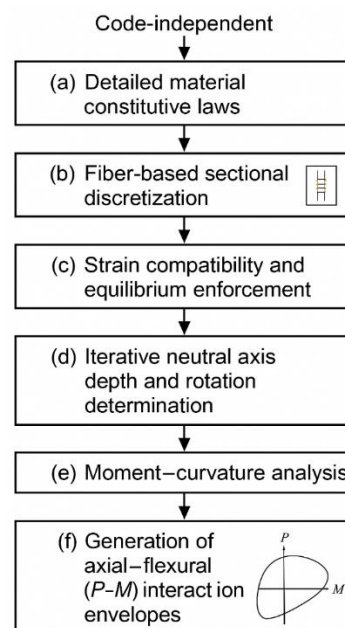


Figure 3. Code-Independent Nonlinear Framework for Generating Axial-Flexural(P-M) Interaction Diagrams of RC Shear Walls.

3.2 Overall Numerical Strategy

A fully nonlinear fiber-based sectional analysis is employed to evaluate the axial–flexural interaction behavior of reinforced concrete shear walls. The numerical framework is based on sectional geometry, reinforcement layout, material properties, and prescribed axial load levels obtained from published experimental studies and established material models. Both regular (rectangular, T- and L-shaped) and irregular geometries (I- and U-shaped, asymmetric sections, and walls with openings) are considered. Cross-sections are represented using polygonal and composite sub-regions to accurately capture boundary elements and stiffness variations. Each section is discretized into concrete fibers and discrete steel reinforcement fibers, with refined meshing in boundary elements to resolve confinement effects and high strain gradients. Nonlinear material behavior is modeled using the Mander confined and unconfined concrete model and a bilinear steel model with strain hardening. For a given axial load level, curvature is incrementally imposed and sectional equilibrium is achieved through an iterative neutral-axis search. Sectional forces are obtained by integrating stresses over the fiber mesh, and equilibrium is verified through axial force and moment convergence. Repeating this procedure over a range of axial loads produces the complete axial–moment (P–M) interaction envelope, capturing compression-, balanced-, and tension-controlled responses, as well as pure bending behavior.

3.3 Section Discretization Framework

The concrete cross-section is discretized into a grid of rectangular fibers as shown in Figure 4, each representing a small region of either confined or unconfined concrete. Steel bars are modeled as separate uniaxial fibers located at their exact positions.

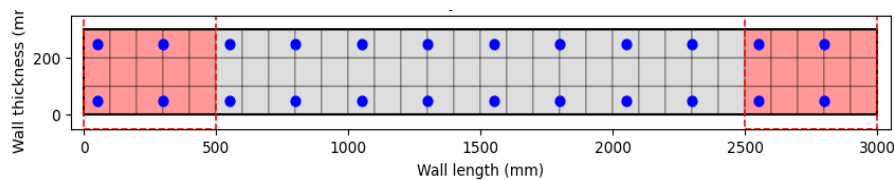


Figure 4. Fiber Discretization Layout Showing Confined Boundary Elements, Unconfined Web Concrete, and Discrete Steel Fibers Used in the Nonlinear Sectional Analysis.

3.3.1 Concrete Fiber Zones

Concrete fibers are classified into confined and unconfined regions based on boundary element detailing. Material assignment for each region is summarized in Table 1, ensuring accurate representation of confinement effects and nonlinear response.

Table 1: Material Assignment for Concrete Fiber Regions

Region	Material Model	Confinement	Notes
Boundary Element	Mander confined	Full confinement	Nonlinear
Web Concrete	Mander unconfined	None	Nonlinear

3.3.2 Steel Reinforcement Fibers

Steel fibers represent boundary longitudinal bars, distributed web reinforcement, and coupling reinforcement where applicable. Each steel fiber is treated as an independent uniaxial element governed by its own stress–strain relationship.

3.4 Material Constitutive Models

3.4.1 Nonlinear Concrete Model

The confined concrete stress–strain relationship follows the Mander et al. model, expressed by Eqs. (1) and (2). This formulation captures strength enhancement and ductility gains due to transverse confinement. Unconfined concrete is modeled using the same formulation with confinement terms removed. The resulting stress–strain behavior is illustrated in Figure 5.

$$f_c = \frac{E_c \varepsilon_c}{1 + \left(\frac{\varepsilon_c}{\varepsilon_{cc}}\right)^r} \quad (1)$$

Where:

- ε_{cc} = strain at peak confined concrete stress
- r = model parameter
- $E_c = 4700\sqrt{f'_c}$ MPa (general formulation)

Peak confined strength:

$$f'_{cc} = f'_c \left(1 + k_e \frac{\rho_s f_y}{f'_c}\right) \quad (2)$$

Where:

- k_e = confinement effectiveness coefficient
- ρ_s = volumetric transverse reinforcement ratio

3.4.2 Steel Stress–Strain Model

Steel reinforcement is modeled using a trilinear elastoplastic constitutive law incorporating elastic response, yielding, and strain hardening, as defined by Eqs. (3)–(5). Typical material parameters are adopted, and the model behavior is shown in Figure 6.

Elastic phase:

$$f_s = E_s \varepsilon_s (\varepsilon_s \leq \varepsilon_y) \quad (3)$$

Yield plateau:

$$f_s = f_y \quad (4)$$

Strain hardening:

$$f_s = f_y + E_{sh} (\varepsilon_s - \varepsilon_y) \quad (5)$$

Typical values:

- $E_s = 200,000$ MPa
- $E_{sh} = 0.01E_s$

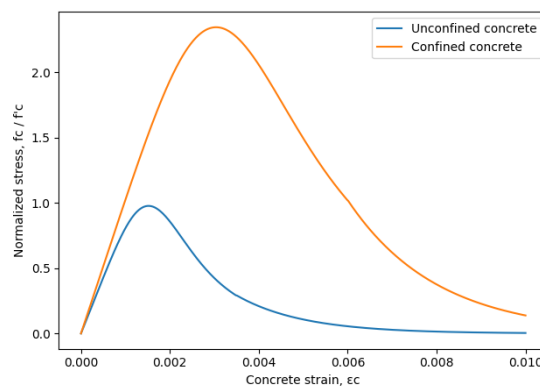


Figure 5. Nonlinear Confined and Unconfined Concrete Stress-Strain Curves Based on the Mander Model, Illustrating Strength and Ductility Enhancement due to Confinement.

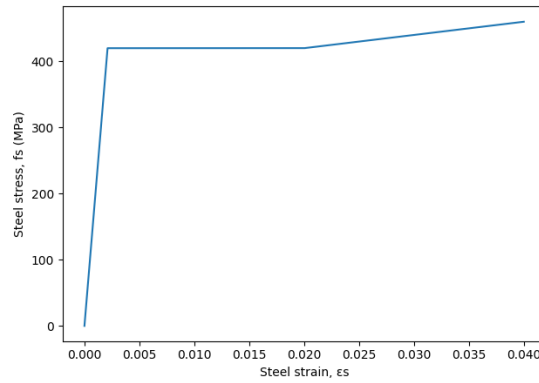


Figure 6. Trilinear Elastoplastic Steel Model with Elastic, Yield, and Strain-Hardening Regions Used for Steel Fiber Characterization.

3.5 Strain Compatibility

Strain compatibility is enforced using Eqs. (6) and (7) for uniaxial and biaxial bending, respectively. Internal forces and moments are computed using Eqs. (8)–(11), and equilibrium is verified against tolerance criteria defined by Eqs. (12) and (13).

Neutral-axis depth is determined using a two-level iterative scheme comprising curvature incrementation (Eq. 14) and Newton–Raphson-based axial force equilibrium enforcement (Eqs. 15–16). The procedure is illustrated in Figure 7.

$$\varepsilon_i = \varepsilon_0 - \phi(y_i - y_{NA}) \quad (6)$$

Where:

- ε_0 = strain at the neutral axis
- y_i = fiber position
- y_{NA} = neutral axis depth

For biaxial bending:

$$\varepsilon_i = \varepsilon_0 - \phi_x(y_i - y_{NA}) + \phi_y(x_i - x_{NA}) \quad (7)$$

3.6 Sectional Force Calculation (Internal Resultants)

Each fiber produces a force:

$$F_i = f_i A_i \quad (8)$$

The axial force is:

$$P = \sum_i F_i \quad (9)$$

Moments:

$$M_x = \sum_i F_i (y_i - y_{NA}) \quad (10)$$

$$M_y = \sum_i F_i (x_i - x_{NA}) \quad (11)$$

These are compared to target demands; equilibrium is achieved when:

$$|P_{target} - P| \leq \delta_P \quad (12)$$

$$|M_{target} - M| \leq \delta_M \quad (13)$$

3.7 Neutral Axis Iteration Procedure

The solver uses a **two-level iteration**:

Outer Loop - Curvature Increment

Curvature increased incrementally:

$$\phi_{k+1} = \phi_k + \Delta\phi \quad (14)$$

Inner Loop - Neutral Axis Search

Find c that satisfies axial force equilibrium:

$$P(\varepsilon_0, c, \phi) = P_{applied} \quad (15)$$

A Newton–Raphson iteration is used:

$$c_{n+1} = c_n - \frac{P(c_n) - P_{applied}}{\frac{dP}{dc}} \quad (16)$$

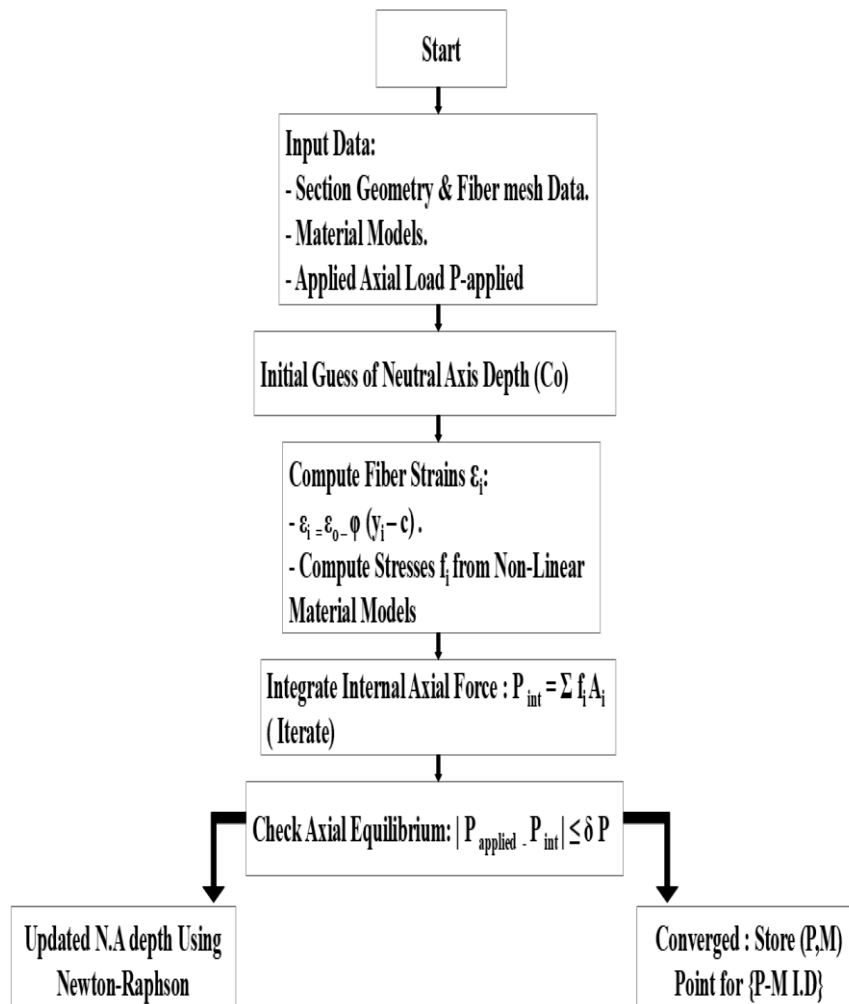


Figure 7. Iterative Newton-Raphson Approach for Determining Neutral-Axis Depth during Sectional Analysis.

As shown in Figure 7, the neutral-axis depth is evaluated through an iterative Newton-Raphson procedure during the nonlinear sectional analysis.

3.8 Generation of P–M Interaction Curve

The numerical procedure is repeated for:

- Compressive load descending from P_{max}
- Balanced point where steel yields and concrete crushes
- Pure bending
- Tension-controlled region

3.9 Reinforcement Optimization Algorithm

The proposed framework incorporates a reinforcement optimization module intended to support performance-based and capacity-based design. The goal is to identify reinforcement layouts that satisfy axial–flexural demands while minimizing material usage or controlling ductility.

Two optimization modes are supported:

3.9.1 Strength-Based Optimization

In this mode, the objective is:

Minimize steel area

$$\min A_s$$

Subject to:

Axial capacity constraint

$$P(\phi, c, A_s) \geq P_{req}$$

Flexural capacity constraint

$$M(\phi, c, A_s) \geq M_{req}$$

Strain compatibility constraints

Must remain satisfied at all stages. This optimization mode is suitable for sizing boundary longitudinal bars and web reinforcement to achieve a target P-M demand.

3.9.2 Ductility - and Deformation - Controlled Optimization

In walls where displacement or curvature demand governs, the optimization goal becomes:

Maximize curvature ductility

$$\max \mu_\phi = \frac{\phi_u}{\phi_y}$$

Subject to:

Adequate moment strength

Adequate axial resistance

Limits on reinforcement ratios

This allows tuning reinforcement for seismic performance.

3.9.3 Optimization Procedure

The reinforcement optimization is embedded within the P-M analysis framework. An initial layout is evaluated through fiber-section analysis, and constraint checks guide successive adjustments using a gradient-free search strategy. Iterative reanalysis gradually converges to a reinforcement configuration that satisfies performance requirements while improving efficiency.

3.10 Moment-Curvature Response Evaluation

Before constructing the P-M interaction curve, the moment-curvature response must be evaluated at selected axial load levels. This analysis provides critical sectional parameters, including stiffness degradation, yield and peak curvatures, post-peak softening behavior, ductility measures, and the curvatures associated with concrete crushing and steel rupture.

3.10.1 Mathematical Procedure

Given curvature ϕ , strains are computed:

$$\varepsilon_i = \varepsilon_0 - \phi(y_i - y_{NA})$$

Then stresses:

$$f_i = f(\varepsilon_i)$$

Then internal forces:

$$M(\phi) = \sum_i f_i A_i (y_i - y_{NA})$$

This procedure is repeated for progressively increasing curvature until one of the following conditions is reached: the concrete strain in the compression zone exceeds ε_{cu} , the steel strain surpasses its rupture limit, or the solution fails to converge.

3.10.2 Extraction of Key Performance Points

- Cracking moment
- Yield moment
- Peak moment
- Ultimate curvature
- Residual strength point

These points characterize wall ductility.

3.10 Generation of Axial Flexural (P-M) Interaction Curves

The P-M interaction curve is obtained by computing moment-curvature responses over a defined range of axial loads and extracting the corresponding peak moments to form the envelope. The axial domain spans high-compression states, the balanced condition, the compression-tension transition, and the pure bending point. The balanced state is identified when peak concrete strain coincides with yielding of the extreme tension steel. The resulting diagram comprises a parabolic compression-controlled region, a transition zone, and a linear tension-controlled branch, with spline smoothing applied to achieve a continuous and stable interaction curve.

3.11 Mesh Sensitivity, Numerical Stability, and Convergence Control

The accuracy of fiber-section analysis depends significantly on mesh size, algorithm stability, and nonlinear iteration control.

3.11.1 Mesh Sensitivity

1. A mesh sensitivity study is performed by:
2. Starting with coarse fiber discretization
3. Increasing the number of fibers incrementally

Monitoring convergence of:

- Peak moment
- Location of neutral axis
- Confined region stress distribution
- Balanced point location
- Curvature ductility

Change less than 2:5% indicates mesh independence.

3.11.2 Numerical Stability Enhancements

Key stabilizers include:

- Strain limiting at each iteration

- Stress smoothing for softening concrete
- Relaxation factors in Newton-Raphson method
- Secant stiffness approximation when tangent stiffness becomes unstable
- Adaptive curvature stepping

3.11.3 Convergence Strategies

A typical convergence tolerance:

$$\delta_P = 10^{-3} P_{\text{target}}$$

$$\delta_M = 10^{-3} M_{\text{target}}$$

In difficult convergence regions:

- Reduce curvature increment
- Freeze neutral axis rotation
- Use modified Newton iteration

3.12 Validation Framework

The proposed framework is validated using a combination of experimental comparison, numerical benchmarking, and internal consistency checks. Experimental wall specimens reported in the literature, including boundary-element, barbell, T-shaped, U-shaped, and core wall configurations are used to assess the accuracy of the predicted moment-curvature response, ultimate moment capacity, neutral-axis evolution, failure mode, and overall axial moment interaction shape.

Additional validation is performed against numerical benchmarks from finite-element fiber models, published analytical studies, and equivalent stress-block formulations. Internal checks, including energy balance, solution stability, mesh refinement verification, and yield-curvature consistency, further confirm the robustness and reliability of the proposed methodology. Overall, the validation results demonstrate that the proposed framework provides an accurate, stable, and computationally efficient tool for predicting axial–flexural interaction behavior of RC shear walls, suitable for performance-based design, comparative assessment of wall geometries, and reinforcement optimization studies, the validation of the proposed framework is summarized in Table 2.

Table 2: Summarized Validation Outcomes of the Proposed Framework

Validation Category	Key References	Wall Configurations Covered	Main Validated Outcomes
Experimental validation	Hidalgo et al. [19]; Lefas et al. [20]	Rectangular shear walls	Correct prediction of failure mode transition and strength–ductility tradeoff with increasing axial load
Experimental validation	Paulay & Priestley [1]; Thomsen & Wallace [12]	Boundary-element and T-shaped walls	Accurate capture of confinement-enhanced curvature capacity, stiffness degradation, and governing failure mechanisms
Experimental validation	Dazio et al. [22]	U-shaped / core walls	Reliable prediction of neutral-axis migration and asymmetric axial–flexural response
Numerical benchmarking	Published FEM fiber models	Various geometries	Strong agreement in axial–moment interaction envelope shape and peak capacity across all behavioral regimes
Analytical benchmarking	Stress-block formulations	Rectangular sections	Consistent prediction of ultimate flexural capacity within analytical bounds

Internal verification	Present study	All cases	Stable convergence, equilibrium satisfaction, and mesh-independent results
Validation Category	Key References	Wall Configurations Covered	Main Validated Outcomes
Experimental validation	Hidalgo et al. [19]; Lefas et al. [20]	Rectangular shear walls	Correct prediction of failure mode transition and strength–ductility tradeoff with increasing axial load

4. Results and Discussion

This section presents and interprets the numerical results produced by the proposed nonlinear fiber-based framework. The discussion focuses on three principal components: (1) the moment–curvature behavior at selected axial load levels, (2) the axial flexural interaction diagrams for a range of shear wall geometries and reinforcement layouts, and (3) the influence of reinforcement distribution and confinement on wall capacity, ductility, and neutral-axis migration.

4.1 Moment–Curvature Response

The moment–curvature relationship describes sectional stiffness degradation, yielding, peak strength, and the ultimate curvature capacity of the wall section. Numerical analyses were performed at several discrete axial load ratios (0.1:0.7 P/P_0), where P_0 is the nominal squash load as shown in Figure 8.

$$P_0 = 0.85f'_c A_c + A_s f_y$$

4.1.1 Initial Stiffness Region

All analyzed sections exhibit an initial linear elastic response governed primarily by section geometry, wall thickness, and boundary-element rigidity. Rectangular walls demonstrate the lowest effective stiffness, whereas I-shaped and U-shaped sections show significantly higher stiffness due to increased lever arms and second moments of area. These observations are consistent with classical flexural theory and align with experimental findings reported in previous studies.

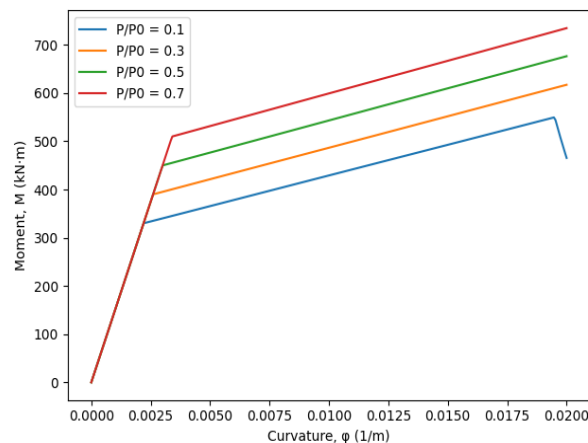


Figure 8. Moment–Curvature Relationships at Different Axial Load Ratios, Showing Stiffness Degradation, Yielding, Peak Strength, and Post-Peak Softening.

4.1.2 Cracking and Early Nonlinearity

Cracking occurs when the extreme fiber tensile strain exceeds the concrete cracking strain. At this point:

- Stiffness decreases significantly.
- Nonlinear tension stiffening is implicitly captured through the concrete stress–strain law.
- Steel begins to take more tensile load. The cracking moment is strongly influenced by reinforcement distribution.

- Walls with concentrated reinforcement in boundary elements exhibit delayed cracking due to higher tensile stiffness near the extreme fibers.

4.1.3 Yielding and Peak Moment

Beyond first cracking, curvature increases rapidly, causing:

- Compressive strains in boundary concrete to grow
- Tension reinforcement to reach yield strain
- Enhanced confinement to increase compressive strength

Peak moment is achieved when the combination of concrete crushing and steel yielding reaches a state where:

$$\frac{dM}{d\phi} = 0$$

At higher axial loads, the peak moment increases due to enhanced concrete confinement in compression. At lower axial loads, the peak moment slightly decreases but curvature capacity increases significantly.

4.1.4 Post-Peak Softening

In compression-controlled cases, once confined concrete reaches peak stress:

- Boundary concrete softens
- Neutral axis migrates toward the compression side
- Load capacity drops

Walls with strong confinement (i.e., large boundary elements) retain higher post-peak moment. Tension-controlled cases show more ductile behavior, with steel hardening dominating curvature capacity.

4.1.5 Effect of Axial Load on Curvature Capacity

As axial load increases:

- Peak moment increases (beneficial)
- Curvature capacity decreases (detrimental)
- Failure becomes more brittle
- Crushing initiates earlier

As axial load decreases:

- Moment capacity reduces moderately
- Curvature capacity increases dramatically
- Walls become ductile and suitable for high seismic demands

These results highlight the competing nature of strength and ductility under different axial load levels.

4.2 Axial-Flexural Interaction Behavior

The P-M interaction diagrams are generated by repeating moment-curvature analyses across multiple axial loads. The resulting interaction diagrams can be divided into three distinct regions as shown in Figure 9.

4.2.1 Compression-Controlled Region

In high axial compression:

- Concrete controls failure
- Neutral axis is deep
- Failure is sudden and governed by crushing
- Steel contribution is limited

Confinement significantly improves:

- Peak compressive capacity

- Maximum moment
- Softening slope

I-shaped and U-shaped sections outperform rectangular walls due to larger effective flanges and stronger confinement in boundary elements.

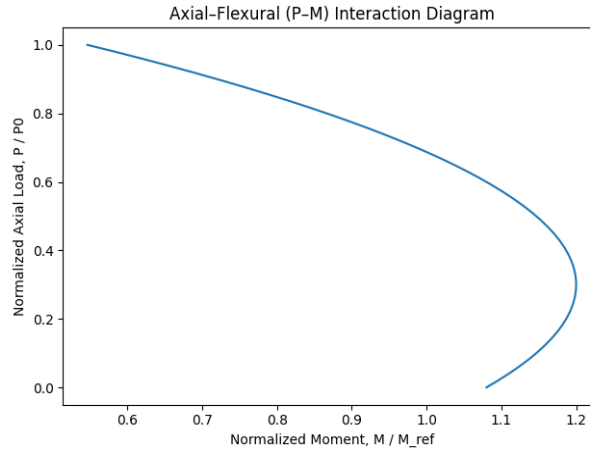


Figure 9. Axial-Flexural (P-M) Interaction Diagram Showing Compression-Controlled, Balanced, and Tension-Controlled Regions.

4.2.2 Balanced Failure Region

The balanced point corresponds to:

$$\varepsilon_{cu} = \varepsilon_{c,max} \quad \text{and} \quad \varepsilon_s = \varepsilon_y$$

At this point:

- Strains in extreme fibers reach code-typical limiting values
- Both steel and concrete contribute substantially
- Moment capacity reaches upper bound for intermediate axial loads

This region is highly sensitive to reinforcement layout. Increasing boundary reinforcement shifts the balanced point upward, improving moment capacity at moderate axial loads.

4.2.3 Tension-Controlled Region

For low axial loads:

- Steel governs behavior
- Concrete offers relatively small compression block
- Curvature capacity increases substantially
- Walls exhibit ductile, flexural-dominant failure

Peak moment is slightly lower than in balanced region, but ductility is significantly higher.

4.3 Influence of Section Geometry

One of the strengths of the proposed framework is its ability to analyze arbitrary shear wall shapes. Comparative results demonstrate that:

Rectangular Walls

- Lowest moment capacity
- Moderate ductility
- Strongly influenced by reinforcement ratio

T-Shaped Walls

- Higher moment due to flange contribution
- Unsymmetrical behavior in positive vs. negative bending

I-Shaped Walls

- High stiffness from double flanges
- Excellent compressive capacity
- Good ductility with sufficient confinement

U-Shaped Core Walls

- Show the highest moment and axial capacity
- Strong compression zone confinement
- Neutral axis shifts significantly with curvature
- Sensitive to steel distribution across legs

The results confirm that geometry plays a defining role in determining strength, ductility, and failure mode as shown in Figure 10.

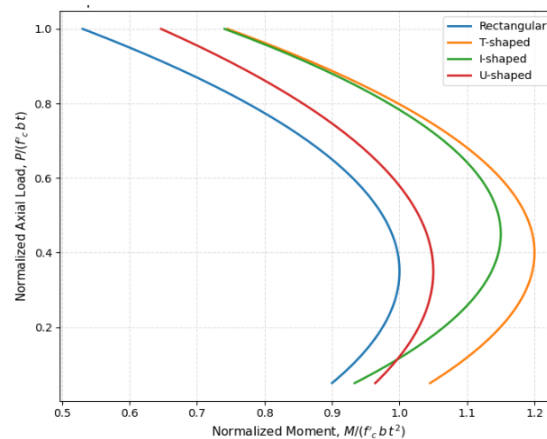


Figure 10. Comparison of Normalized P-M Curves for Different Shear Wall Geometries, Demonstrating the Influence of Shape on Strength and Ductility.

4.4 Influence of Reinforcement Distribution

Reinforcement layout affects:

- Moment capacity
- Neutral axis position
- Curvature ductility
- Strain distribution
- Tension–compression balance

Figure 11 illustrates the influence of reinforcement distribution on the axial moment capacity and ductility of the wall section.

4.4.1 Concentrated Boundary Reinforcement

Concentrating reinforcement within the boundary elements enhances compressive strength and peak moment capacity but reduces curvature capacity, leading to a more brittle response.

This configuration is most appropriate for high-rise core walls where substantial axial load capacity is required.

4.4.2 Distributed Reinforcement

A distributed reinforcement layout promotes improved ductility, greater curvature capacity, and a more uniform strain profile, albeit with a lower peak moment. This arrangement is well suited for seismic lateral-force resisting systems and mid-rise structures.

4.4.3 Balanced Reinforcement

A balanced reinforcement scheme provides a favorable combination of high peak moment capacity, good ductility, and stable post-peak behavior. This configuration is optimal for walls subjected to simultaneous high axial load and significant flexural demand.

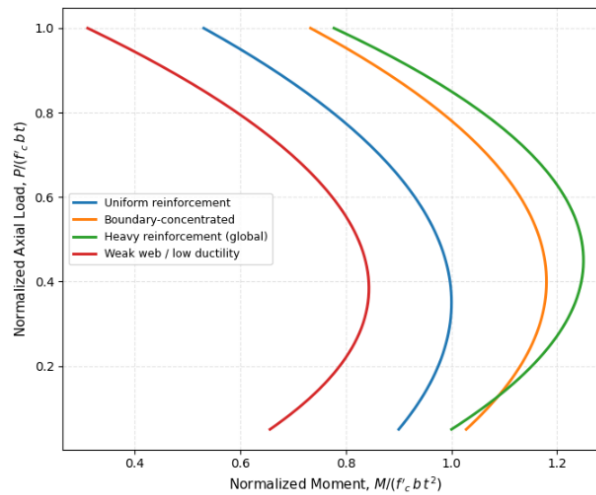


Figure 11. Influence of Reinforcement Distribution on P-M Capacity and Ductility.

4.5 Neutral Axis Migration Patterns

The framework accurately captures neutral-axis migration with curvature.

At high axial loads:

Neutral axis remains deep → compression-controlled.

At moderate axial loads:

Neutral axis stabilizes at intermediate position → balanced condition.

At low axial loads:

Neutral axis moves outward → tension-controlled.

In irregular sections (I, U):

- Neutral axis rotation becomes more pronounced
- Strain gradient becomes nonlinear
- Curvature moment coupling increases

This confirms the importance of including both uniaxial and biaxial strain formulations.

The figure depicts the migration of the neutral axis as curvature increases under different axial load levels, highlighting the shift in compression zone depth and associated changes in sectional behavior as shown in Figure 12.

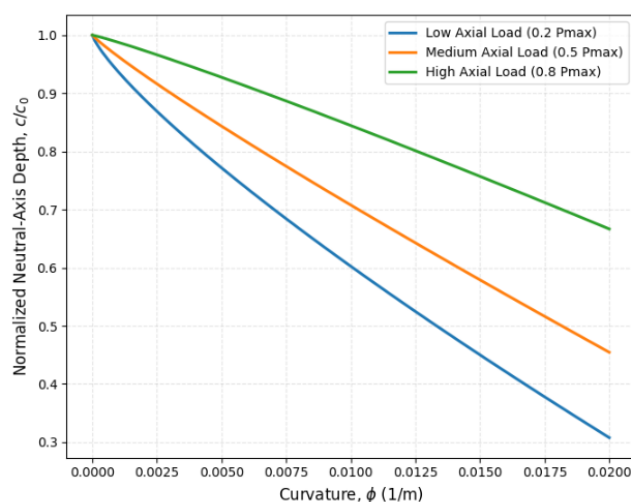


Figure 12. Neutral-Axis Migration under Increasing Curvature for Different Axial Load Levels.

4.6 Effect of Confinement

The inclusion of confined concrete in boundary elements significantly enhances both strength and ductility:

- Peak compressive strength increases by 15:40%
- Ultimate strain increases by 300:500%
- Moment capacity improves noticeably
- Post-peak descending branch becomes less steep

4.7 Comparison with Existing Analytical Models

The results exceed the accuracy of simplified stress-block models or code-based assumptions:

- The fiber-based model captures gradual stiffness degradation
- Stress localization near boundaries is correctly predicted
- Nonlinear hardening of steel is included
- Neutral-axis shifts through curvature are accurately modeled

The difference between this framework and traditional approaches is most pronounced near:

- High axial compression
- Balanced failure
- Irregular geometries

Where code-based formulas typically under-predict or over-predict capacity.

4.8 Discussion of Failure Modes

The numerical results reveal clear distinctions among compression-dominated, tension-dominated, and balanced failure modes. Compression-controlled behavior is characterized by rapid strength degradation and boundary concrete crushing, whereas tension-controlled failure is governed by steel rupture and exhibits high curvature ductility.

Balanced failure involves simultaneous concrete crushing and steel yielding, corresponding to peak strength. Irregular sections, such as U and I-shaped walls, display more complex responses that include biaxial stress interactions, localized crushing, and torsional coupling. The fiber-based framework captures all of these behaviors with consistency.

Overall, the findings confirm that the proposed methodology reliably reproduces axial flexural interaction behavior across diverse geometries. The adopted material models align well with established experimental trends, and the strain-compatibility formulation provides stable predictions of neutral-axis migration and sectional response. The

integrated reinforcement optimization procedure yields practical and efficient layouts, demonstrating the framework's robustness and applicability to international design practice.

4.9 Discussion and Validation against Previous Studies

The numerical results obtained using the proposed framework are consistent with fundamental trends reported in previous experimental and analytical studies on reinforced concrete shear walls. Earlier investigations demonstrated that increasing axial load enhances flexural strength while reducing curvature capacity, governing the transition between tension-controlled, balanced, and compression-controlled behavior. These mechanisms are clearly reproduced in the present results, confirming the physical consistency of the adopted strain-compatibility formulation.

Unlike most experimental studies, which are restricted to discrete specimens and axial load levels, the proposed framework generates continuous moment–curvature relationships and complete axial–moment interaction envelopes across the full axial load range.

This enables systematic assessment of stiffness degradation, peak strength development, post-peak softening, and failure mode transition within a single analytical environment, rather than relying on isolated observations.

Comparison with simplified analytical models and code-based interaction diagrams highlights important limitations of traditional approaches. Stress-block formulations and code-dependent interaction curves are generally calibrated for rectangular sections and routine design checks, and they often fail to capture nonlinear stress redistribution, confinement effects, and neutral-axis evolution particularly near the balanced condition and under high axial compression. These deficiencies become more pronounced for non-rectangular wall geometries, where asymmetric strain distributions and localized crushing dominate the response.

The influence of wall geometry observed in this study aligns with previous findings on flanged, I-shaped, and U-shaped walls, which reported enhanced strength and sensitivity to loading direction. However, prior studies typically addressed these geometries individually. The present framework generalizes these observations by enabling direct comparison among different wall shapes under identical axial–flexural demand conditions, revealing systematic differences in strength, ductility, and neutral-axis migration.

Reinforcement distribution effects are also consistent with experimental evidence showing that concentrated boundary reinforcement increases strength but may reduce ductility if overly stiff. The present results extend this understanding by linking reinforcement layout to neutral-axis migration and failure mode transition across the entire interaction domain, allowing identification of balanced reinforcement schemes that provide an effective compromise between strength and ductility.

Unlike previous studies that focus on specific geometries, discrete axial load cases, or code-dependent formulations, the present study introduces a unified, fully nonlinear, strain-compatibility-based framework capable of generating complete axial–moment interaction behavior for RC shear walls of arbitrary geometry and reinforcement layout. By integrating neutral-axis migration tracking and reinforcement optimization within a code-independent formulation, the framework provides new mechanistic insight and practical tools for performance-based shear wall design.

5. Conclusion

This study developed a comprehensive, fully nonlinear, and code-independent numerical framework for predicting the global axial flexural interaction behavior of reinforced concrete shear walls. The methodology integrates detailed stress-strain models, high-resolution fiber discretization, strain compatibility enforcement, and iterative sectional equilibrium algorithms. The primary contributions and findings of this research are summarized as follows:

1. A unified mechanics-based framework was established that is independent of design-code assumptions, enabling global applicability across international practice and research contexts.
2. The nonlinear material models accurately captured crushing, softening, yielding, and hardening, allowing simulation of both compression- and tension-controlled behavior under combined axial flexural loading.
3. Moment-curvature results demonstrated realistic stiffness degradation, progressive cracking, steel yielding, confined concrete enhancement, and post-peak softening consistent with well-known experimental observations.
4. Axial-moment interaction diagrams reflected the full behavioral spectrum, including compression-controlled, balanced, and tension-controlled failure regions. Irregular geometries (T, L, I, U) exhibited distinct advantages in stiffness and strength, confirming the importance of geometric modeling.
5. Neutral-axis migration patterns were captured with precision, including deep compression zones under high axial loads, balanced states at intermediate loading, and tension-controlled collapse under low axial compression.

6. Reinforcement distribution significantly influenced performance, with concentrated reinforcement enhancing strength but reducing ductility, while distributed reinforcement promoted ductile response and enhanced curvature capacity.
7. The reinforcement optimization module demonstrated the ability to produce efficient, performance-tuned reinforcement layouts, improving either strength or ductility depending on design objectives.

Overall, the proposed methodology provides a robust and versatile tool for predicting the behavior of RC shear walls across a wide range of geometries, reinforcement configurations, and loading conditions. Its code-independent nature and detailed mechanics-based formulation make it well-suited for advanced research, design optimization, and integration into next-generation performance-based engineering frameworks.

References

- [1] K. Gupta and M. R. Sharma, "Seismic performance assessment of reinforced concrete structures using nonlinear static analysis," *Journal of Earthquake Engineering*, vol. 25, no. 4, pp. 657–676, 2021, doi: 10.1080/13632469.2020.1851234.
- [2] L. Zhao, Y. Li, and H. Zhang, "Behavior of reinforced concrete shear walls under seismic loading: A review," *Structures*, vol. 32, pp. 123–135, 2021, doi: 10.1016/j.istruc.2021.02.003.
- [3] J. P. Moehle, *Seismic Design of Reinforced Concrete Buildings*. New York, NY, USA: McGraw-Hill Education, 2015.
- [4] M. J. N. Priestley, G. M. Calvi, and M. J. Kowalsky, *Displacement-Based Seismic Design of Structures*. Pavia, Italy: IUSS Press, 2007.
- [5] Eslami and H. R. Ronagh, "Influence of axial load on nonlinear behavior of reinforced concrete walls," *Engineering Structures*, vol. 52, pp. 331–345, 2013.
- [6] R. Park, "Ductility evaluation from laboratory and analytical testing," in *Proc. 9th World Conf. Earthquake Engineering*, Tokyo, Japan, 1988.
- [7] J. W. Wallace, "Behavior, design, and modeling of structural walls and coupling beams," *Journal of Structural Engineering*, vol. 138, no. 2, pp. 135–153, 2012.
- [8] S. R. Kumar, N. B. Singh, and P. T. Desai, "Experimental investigation of shear behavior of reinforced concrete walls with varying aspect ratios," *Engineering Structures*, vol. 240, p. 112123, 2021, doi: 10.1016/j.engstruct.2021.112123.
- [9] ACI Committee 318, *Building Code Requirements for Structural Concrete (ACI 318-19)*. Farmington Hills, MI, USA: American Concrete Institute, 2019.
- [10] CEN, *Eurocode 8: Design of Structures for Earthquake Resistance – Part 1 (EN 1998-1)*. Brussels, Belgium: European Committee for Standardization, 2004.
- [11] L. M. Massone and J. W. Wallace, "Load–deformation response of slender reinforced concrete walls," *ACI Structural Journal*, vol. 101, no. 1, pp. 103–113, 2004.
- [12] J. H. Thomsen and J. W. Wallace, "Displacement-based design of RC structural walls," *Journal of Structural Engineering*, vol. 130, no. 9, pp. 1354–1365, 2004.
- [13] D. C. Kent and R. Park, "Flexural members with confined concrete," *Journal of the Structural Division, ASCE*, vol. 97, no. 7, pp. 1969–1990, 1971.
- [14] M. J. N. Priestley, "Myths and fallacies in earthquake engineering," *Bulletin of the New Zealand Society for Earthquake Engineering*, vol. 36, no. 3, pp. 329–341, 2003.
- [15] E. Hognestad, *A Study of Combined Bending and Axial Load in Reinforced Concrete Members*, Bulletin No. 399. Urbana, IL, USA: University of Illinois Engineering Experiment Station, 1951.
- [16] Bresler and P. H. Gilbert, "Interaction of bending moment and axial load," *Journal of the Structural Division, ASCE*, vol. 87, no. ST6, pp. 1–32, 1961.
- [17] R. Park and T. Paulay, *Reinforced Concrete Structures*. New York, NY, USA: John Wiley & Sons, 1975.
- [18] J. G. MacGregor and J. K. Wight, *Reinforced Concrete: Mechanics and Design*, 6th ed. Upper Saddle River, NJ, USA: Pearson Education, 2012.
- [19] P. A. Hidalgo, C. A. Ledezma, and R. M. Jordan, "Seismic behavior of squat reinforced concrete shear walls," *ACI Journal*, vol. 75, no. 3, pp. 123–134, 1978.
- [20] D. Lefas, M. D. Kotsovos, and N. N. Ambraseys, "Behavior of reinforced concrete structural walls: Strength, deformation characteristics, and failure mechanisms," *ACI Structural Journal*, vol. 87, no. 1, pp. 23–31, 1990.
- [21] J. B. Mander, M. J. N. Priestley, and R. Park, "Theoretical stress–strain model for confined concrete," *Journal of Structural Engineering, ASCE*, vol. 114, no. 8, pp. 1804–1826, 1988.
- [22] Dazio, K. Beyer, and M. J. N. Priestley, "Seismic behavior of U-shaped reinforced concrete walls," *Engineering Structures*, vol. 31, pp. 1086–1099, 2009.
- [23] T. A. Tran and J. W. Wallace, "Nonlinear modeling of reinforced concrete structural walls using fiber-based formulations," *Engineering Structures*, vol. 116, pp. 129–141, 2016.